



High-order harmonic generation in a liquid-crystal-like model

Ling-Jie Lü  and Xue-Bin Bian ^{*}

State Key Laboratory of Magnetic Resonance and Atomic and Molecular Physics, Wuhan Institute of Physics and Mathematics, Innovation Academy for Precision Measurement Science and Technology, Chinese Academy of Sciences, Wuhan 430071, China



(Received 6 March 2023; revised 6 May 2023; accepted 31 May 2023; published 10 July 2023)

The ultrafast dynamics of disordered systems have recently garnered considerable interest among researchers. However, due to the inherent complexity of such systems, many critical issues require further elucidation through extensive experimental and simulation data. We conduct calculations on high-order harmonic generation in an anisotropic two-dimensional disordered system that is similar to liquid crystals. Our results demonstrate the characteristics of harmonic spectra with different laser polarization angles and reveal a phenomenon of time delay in harmonic polarization perpendicular to the driving field. We show that this time delay arises from the intermolecular scattering of tunneling electrons before they recombine with holes. Thanks to the discovery of this phenomenon, it is hoped that polarization can be utilized to differentiate the quantum trajectories of high-order harmonics within a subcycle. Our discovery offers a different approach for investigating and manipulating ultrafast electron dynamics in condensed matter, while shedding light on the coherent control of ultrashort light sources.

DOI: [10.1103/PhysRevA.108.013504](https://doi.org/10.1103/PhysRevA.108.013504)

I. INTRODUCTION

The ultrafast electron dynamics induced by ultrashort intense lasers exhibit novel features in both gases and condensed matters [1–6], and the exploration of this field broadens our understanding of extreme nonlinear dynamics and promotes the development of ultrafast detection methods [7–13]. In gases, atoms and molecules can be treated as independent entities during ultrafast processes such as high-order harmonic generation (HHG) [4–6] and strong-field ionization [14–20], but in condensed matter, the electron dynamics are significantly influenced by surrounding electrons and nuclei [9,21]. Especially in a perfect crystal, electrons are nonlocal, this results in distinct characteristics in ultrafast dynamics, such as the double plateau structure [22] and special laser dependence in HHG [9,10,23–27]. When disorder, defects, or doping are introduced into condensed matter, the electron wave functions become localized, exhibiting structures and dynamics distinct from that in crystals and gases. In recent years, ultrafast dynamics in nonperiodic systems such as amorphous solids [28], quasicrystals [29], and liquids [30,31] have attracted considerable attention due to their broad application and research prospects. In these systems, the loss of long-range order leads to the absence of specific energy bands and a departure from the behavior observed in crystals. Unlike the relatively free tunneling electrons in sparse gases, tunneling electrons in disordered system collide with surrounding molecules during the acceleration by laser fields. While the mechanisms of ultrafast dynamics in disordered systems remain unclear, a key question is, what is the effect of intermolecular scattering of tunneling electrons on HHG? Especially for materials with

both disorder and anisotropy, such as liquid crystals, these critical issues are particularly underexplored, and the study in this regard could reveal the role of disorder and localization in HHG.

This paper presents a simulation study of anisotropic disordered systems in two-dimensional space, which share similarities with liquid crystals. Our results show the polarization-angle-resolved high-order harmonic spectra driven by linearly polarized lasers. We observe a time delay in the harmonic radiation perpendicular to the polarization direction of the laser. The in-depth study of this phenomenon gives us an opportunity to distinguish subcycle electron dynamics and quantum trajectories by means of harmonic polarization characteristics. These harmonic characteristics provide insights into the relationship between intermolecular scattering of electrons and harmonic spectra, as well as the impact of this scattering on the recollision model [5,6] in anisotropic disordered systems.

II. METHODS

We constructed a two-dimensional model using the OCTOPUS package [32–34] based on the independent electron approximation. Throughout this paper, we use atomic units (a.u.), unless otherwise specified. The randomness of molecular structure, orientation, and distribution affects the disorder and anisotropy of materials. Collimated linear molecules exhibit typical anisotropy. To describe the potential of a linear molecular ion, we employed three Gaussian functions,

$$V = V_0 \left[e^{-\frac{(x+x_0)^2 + (y+y_0)^2}{\delta^2}} + e^{-\frac{(x+x_0)^2 + (y+y_0+7)^2}{\delta^2}} + e^{-\frac{(x+x_0)^2 + (y+y_0-7)^2}{\delta^2}} \right], \quad (1)$$

where, $V_0 = -0.8$ a.u., $\delta = 1.5$ a.u. describe the depth and width of the potential well, (x_0, y_0) is the central position of

^{*}xuebin.bian@wipm.ac.cn

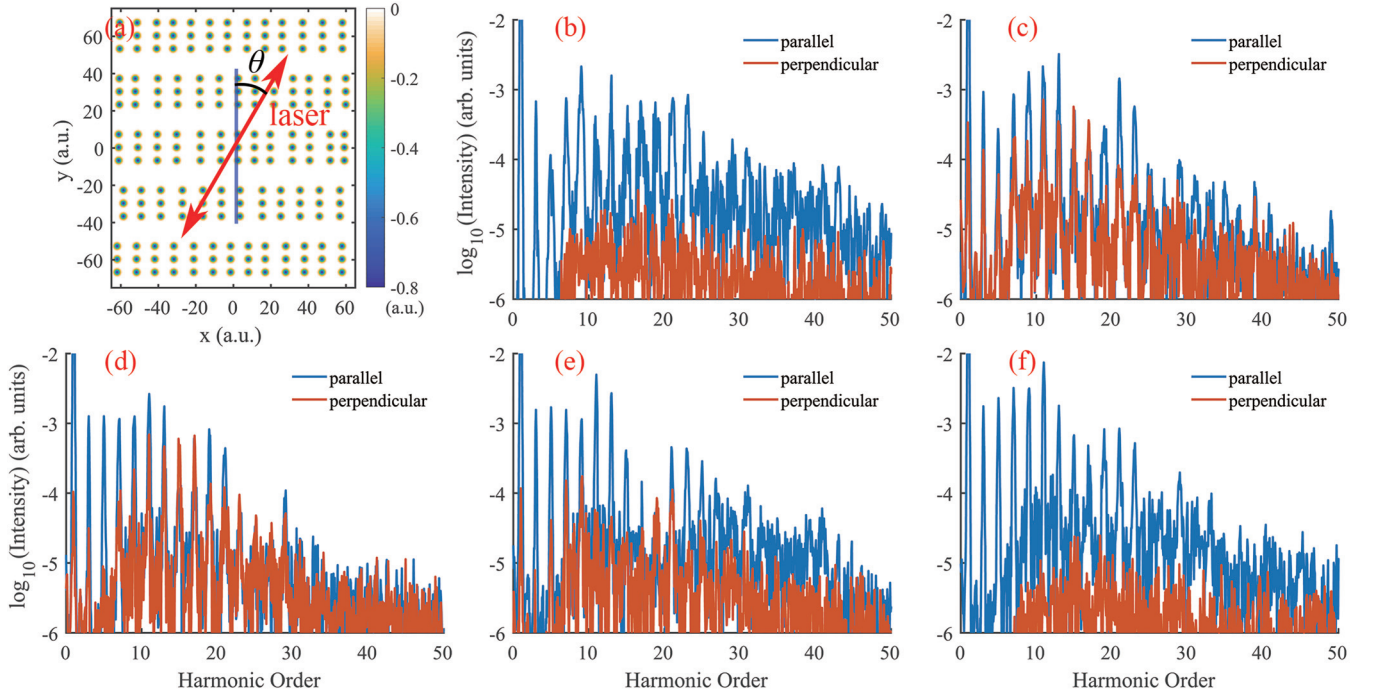


FIG. 1. (a) The ionic potential of our anisotropic disordered model, which is similar to smectic liquid crystals. The angle between the laser polarization direction (indicated by the red double arrow) and the y axis is denoted by θ . The color bar indicates the depth of the potential well. (b)–(f) Harmonic spectra induced by the laser with $\theta = 0, \pi/8, \pi/4, 3\pi/8$, and $\pi/2$, respectively. The blue curves represent the harmonic spectra parallel to the laser polarization direction, and the red curves represent the harmonic spectra perpendicular to the laser polarization direction. The wavelength of the laser is 1500 nm, the peak field strength is 0.03 a.u., and the duration is 16 cycles with a sinusoidal envelope.

the molecule. Obviously, the orientation of the linear molecule is parallel to the y axis, and each atom is separated by 7 a.u. Liquid crystals are classified into various types, according to their formation conditions and molecular arrangement. Among them, smectic liquid crystal is a typical representative, whose molecular arrangement is representative. Inspired by the structural characteristics of smectic liquid crystals, we arrange the molecules into multiple layers. We assume that the distance between each layer is the same along the y direction, while the molecular spacing within each layer is random along the x direction. The interval between each layer is $a_0 = 30$ a.u., and the molecular spacing within the layer is a Gaussian distribution centered on 10 a.u., with standard deviation $\sigma = 1$ a.u. The ionic potential of smectic liquid crystal composed of potential V is shown in Fig. 1(a). In this configuration, 64 molecules are included. Considering the spin, there are six valence electrons in each molecule, so a total of 384 valence electrons are involved in the calculations. To avoid reflection of wave functions at the boundaries, periodic boundaries are utilized at all four sides of the rectangle.

This model shows both disorder and anisotropy through the arrangement and alignment of molecules, which is the characteristic of liquid crystal. We choose the appropriate depth and width of potential well and molecular spacing to make the ionization energy close to that of common liquid crystal molecules in liquid phase [35–37]. We notice that although the simple model potential is difficult to accurately describe the chemical properties of real materials under static state, the interaction between tunneling electrons and parent ions is weak and the interaction between molecules is

random. In this case, we ignore the particularity of molecular structure and pay attention to the general properties of tunneling electron dynamics. The model can give qualitative and semiquantitative results.

III. RESULTS AND DISCUSSIONS

From a macroscopic perspective, we can ignore the symmetry breaking caused by the random fluctuation of molecular arrangement in the x direction. As a result, the layered arrangement of molecules in this model exhibits twofold rotational symmetry, resulting in anisotropy. First, we explore the anisotropy-dependent ultrafast dynamics in the model by using a linearly polarized laser,

$$\vec{E}(t) = f(t)E_0[\hat{x}\sin(\theta) + \hat{y}\cos(\theta)]\cos(\omega t). \quad (2)$$

Here, \hat{x} and \hat{y} are the unit vector in the x and y directions, respectively, $f(t)$ is a sinusoidal envelope with a duration of 16 optical cycles, the peak electric field $E_0 = 0.03$ a.u., the angular frequency $\omega = 0.0304$ a.u. corresponds to an optical period $T = 2\pi/\omega = 5$ fs and a wavelength of 1500 nm. When the angle between laser polarization direction and y axis θ is $0, \pi/8, \pi/4, 3\pi/8$, and $\pi/2$, the harmonic spectra are shown in Figs. 1(b)–1(f). These harmonic spectra exhibit typical odd-order peaks and plateau structures.

In order to show the spectra characteristics more clearly, we integrate the harmonic intensities lower than the 12th order (3rd–11th order) and higher than the 12th order (13th–23rd order), respectively, and show them by curves in Fig. 2. As the angle θ increases, the harmonic intensity higher than the

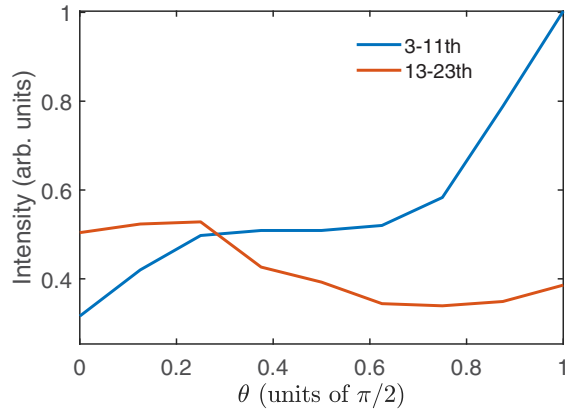


FIG. 2. The blue and red lines show the low-order (3rd–11th) and high-order (13th–23rd) harmonic intensities as a function of the angle θ , respectively.

12th order gradually increases, but the harmonic intensity above 12th order gradually decreases, this is a manifestation of anisotropy during the HHG process. The electrons tunneled out of the molecules are accelerated by the laser field and collide with surrounding molecules. Since the molecules are parallel to the y axis, electrons can pass through the voids between the molecules when they are driven along the y direction, while electrons pass through many molecules when they are driven along the x direction, apparently increasing the probability of scattering, which reduces the probability of recombination, thereby reducing the harmonic intensity in the plateau region. Intermolecular scattering changes the momentum and coherence of electrons, which is similar to the dephasing effect in crystals, resulting in the decrease of harmonic yield in the plateau. In contrast to harmonics higher than the 12th order, the lower-order harmonics come from the nonlinear oscillation of electrons near ions, this may be the reason for the opposite trend of harmonic intensity.

When the monochromatic laser polarization direction is along the x axis [Fig. 1(f)] or the y axis [Fig. 1(b)], the harmonic intensities perpendicular to the polarization direction (red curves) are very low, which are nearly two orders of magnitude lower than that along the parallel direction (blue curves). This indicates that the sampling area is large enough to ignore the effects of fluctuations in the distribution of molecules in the x direction. When the polarization angle θ is between 0 and $\pi/2$, the harmonic intensities perpendicular to the polarization direction increase, even equivalent to that in the parallel direction, when the angle is $\pi/4$ [Fig. 1(d)]. The appearance of perpendicular harmonics is in line with the expectation based on the symmetry of the system, similar to HHG in materials with the same symmetry such as aligned N_2 .

Analysis based on symmetry provides correct predictions, but further analysis is meaningful to reveal the ultrafine dynamics of perpendicular HHG in depth. Therefore, we show the time-frequency analyses [38] of the high-order harmonics with $\theta = \pi/4$ [Fig. 1(d)] in Fig. 3. The time-frequency analyses show quantum orbits, which are similar to those in gas and crystal HHG. A notable feature is that the harmonic radiation time in perpendicular direction is about 1 fs later than that in parallel direction, as marked by a double-headed

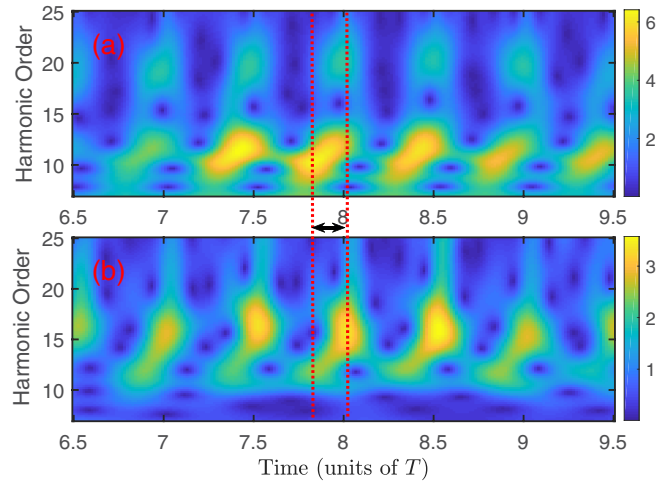


FIG. 3. Time-frequency analyses of the harmonic spectra in Fig. 1(d). (a) parallel to the laser polarization and (b) perpendicular to the laser polarization. The red vertical lines mark the central moments of radiations and the double-headed arrow marks the time delay.

arrow. This HHG mechanism in the perpendicular direction is distinct from the even-order harmonics caused by material symmetry breaking. In fact, this delayed perpendicular harmonic represents a phenomenon that differs from traditional HHG in gases and crystals.

Compared to the coherent motion in sparse gases and crystals, scattering between electrons and other charges in dense disordered systems plays a more significant role in HHG. Tunneling electrons can not only collide with their parent ion and radiate harmonics, but also collide with other ions in the environment and change their momentum. In order to study the effect of scatterings on HHG, we calculate the time-dependent Schrödinger equation (TDSE) in Eq. (3) to simulate the process of quasi-free-electron-ion interaction.

$$i \frac{\partial \psi}{\partial t} = -\frac{1}{2} \left(\frac{\partial^2}{\partial x^2} + \frac{\partial^2}{\partial y^2} \right) \psi + \tilde{V} \psi. \quad (3)$$

\tilde{V} is the potential of a layer of molecules composed of V , which is the third layer in Fig. 1(a), and we use a two-dimensional Gaussian function with a certain velocity as the initial wave function $\psi(t=0) = \psi_0$,

$$\psi_0 = C \exp \left[-\frac{(x-x')^2 + (y-y')^2}{2\delta'^2} + i(k_x x + k_y y) \right], \quad (4)$$

where C is the normalization factor, $\delta' = 14$ a.u. is the full width at half-maximum, $x' = y' = -75$ a.u. is the initial center position, and $k_x = k_y = 0.8$ a.u. is the initial velocity, which is close to the velocity of tunneling electrons driven by the lasers used in this work. We use the split-operator method to evolve the TDSE, and the electron densities at $t = 0.5, 1.5$, and 2.5 fs are shown in Figs. 4(a)–4(c). The expectation values of electron momentums $\langle \psi | \hat{p} | \psi \rangle$ are shown in Figs. 4(d)–4(f) with vector arrows, respectively.

We can see that at the initial time, the electron is free and has an initial velocity with an angle $\pi/4$ relative to the x axis. When electrons collide with molecules, some of the electrons

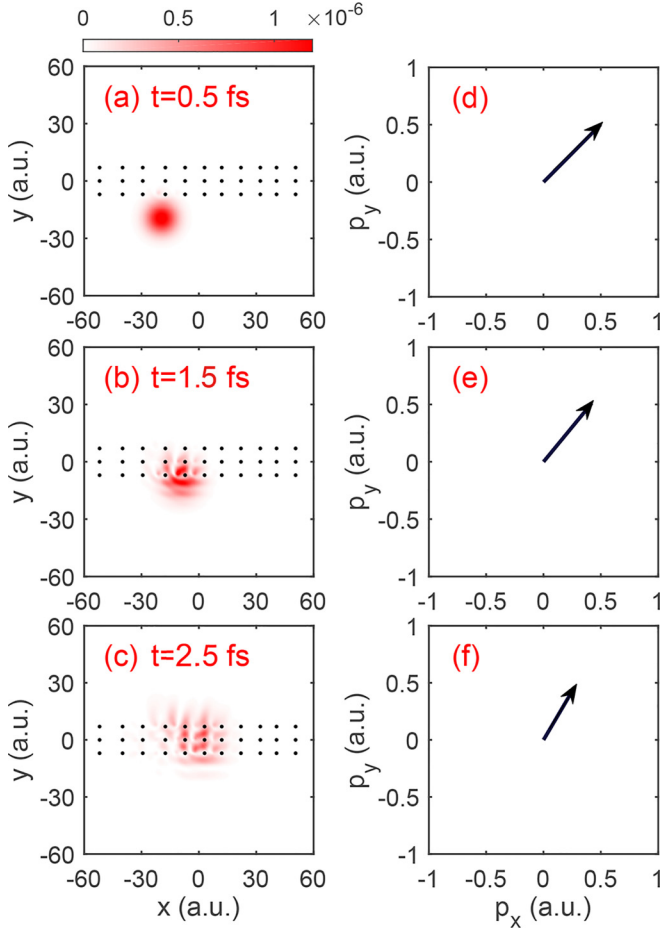


FIG. 4. The red wave packets in (a)–(c) represent electron densities incident on a layer of linear molecules that represented by black dots, and the vector arrows in (d)–(f) are expectations of electron momentum $\langle \psi | \hat{p} | \psi \rangle$, where $t = 0.5, 1.5$, and 2.5 fs, respectively

are scattered. Interestingly, the direction of the expectation of electron momentum deflects, and it deflects nearly $\pi/8$ within 2 fs. These results indicate that tunneled and accelerated electrons interact with surrounding molecules, causing their movement direction to deviate from the direction of laser polarization. This is illustrated in the schematic diagram shown in Fig. 5. Once the direction of the electric vector of the laser is reversed, the electrons slow down and return. The process of returning also experiences the scattering process. According to the symmetry of the system, the returning electrons deflect in the direction of the parent ion and recombine with it. When the electron combines with the parent ion, the velocity of the electron changes by an angle α , which causes the harmonic polarization direction to change as well. Therefore, the deflection of the electron velocity provides the harmonics in the direction perpendicular to the laser polarization. The angle of velocity deflection is larger for electrons that travel longer trajectories, resulting in a predominance of perpendicular harmonics in longer trajectories and parallel harmonics in shorter trajectories. This leads to the radiation time delay shown in Fig. 3. This work provides a means to distinguish and extract femtosecond time-resolved long and short

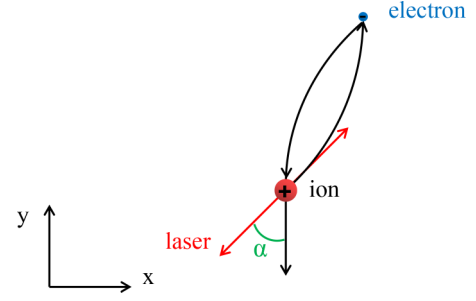


FIG. 5. The red double-headed arrow indicates the laser polarization direction, and the black curves with an arrow indicate the trajectory of tunneling electrons driven by lasers in an anisotropic disordered system. When the electron returns to the parent ion, its velocity is deflected by an angle α .

trajectories using the polarization characteristics of high-order harmonics.

To verify the convergence and robustness of our calculations, we expand the sampling range and choose different configurations of randomly positioned molecules in these calculations, the results remain unchanged qualitatively. In addition, we change the initial position and the initial velocity of the electron wave packet in Fig. 4, and the results are qualitatively unchanged. It should be noted that Berry curvature can also induce perpendicular harmonics in crystals driven by linearly polarized lasers. However, this mechanism is dependent on the band structures and the velocity of deflection is proportional to the laser peak electric field, as shown in previous studies [39,40]. In contrast, the electrons in our simulations are highly localized and the band structures are not present. Additionally, the simulation shown in Fig. 4 does not involve a laser, meaning that the electron's velocity changes once it gains velocity, regardless of the presence of a laser. Therefore, the harmonic generation mechanism discussed in this work is distinct from those reported.

Our interpretation of the time delay in Fig. 3 is based on a recollision model similar to that in gases, and the delay comes from the velocity deflection of returned electrons. On the other hand, for interband harmonics in crystals, the polarization depends on the intrinsic properties of wave functions in the conduction and valence bands, is not aligned with the direction of the group velocity of either electron or hole. This means that the relationship between the group velocity of electron (hole) and the polarization of harmonics is restricted to the intraband model only in crystals. The energy of the intraband radiation is less than the minimum band gap, and is generally considered to have no chirp. This is the reason why harmonic delays are not found in a perfect crystal, although it is anisotropic. Therefore, the phenomenon we reveal is unique to anisotropic disordered systems.

Electrons in disordered systems have similar localization characteristics to electrons in gases, and their motion laws driven by lasers are different from nonlocalized Bloch electrons in crystals. However, the tunneling electrons in gases are almost free when they are far away from the parent ion, and the tunneling electrons in the disordered system are always affected by the molecules in the environment. Our work reveals the impact of these intermolecular interactions on HHG.

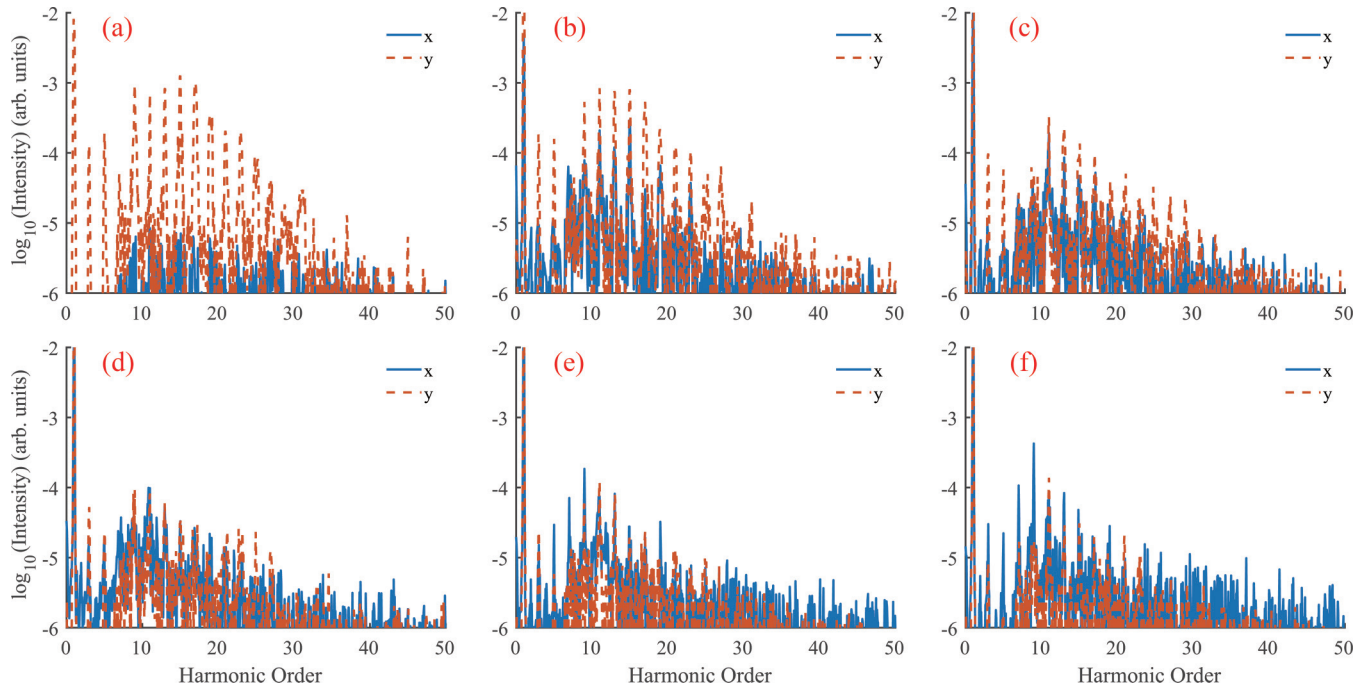


FIG. 6. The laser ellipticity dependence of HHG for the model in Fig. 1(a). The ellipticity ε used in (a)–(f) are 0, 0.2, 0.4, 0.6, 0.8, and 1, respectively. $E_0 = 0.02$ a.u. The wavelength and pulse width are the same as those in Fig. 1. The long axis direction of elliptically polarized laser is along the y direction, and the blue solid and red dotted lines represent the polarization of the harmonics in the x and y directions, respectively.

The trajectories of electrons in anisotropic disordered systems are modified by this impact, which provides an alternative idea for ultrafast control of electron dynamics. This ultrafast controllability of electron velocity provides a different means of controlling the polarization properties of ultrafast light sources.

In addition, we calculate the laser ellipticity dependence of HHG of this model, which is shown in Fig. 6. The laser field is described with ellipticity ε and assumed as a plane wave that travels in the z direction,

$$\vec{E}(t) = f(t) \frac{E_0}{\sqrt{1+\varepsilon^2}} [\hat{x}\varepsilon \cos(\omega t) + \hat{y} \sin(\omega t)]. \quad (5)$$

Harmonic spectra corresponding to $\varepsilon = 0, 0.2, 0.4, 0.6, 0.8$, and 1 are shown in Figs. 6(a)–6(f), respectively. When linearly polarized light is used, harmonics have clear odd-order peaks and an obvious plateau. With the increase of ellipticity, the harmonics in the plateau area are weakened. We integrate the harmonic intensities of the 3rd–23rd orders and show them in Fig. 7. According to the semiclassical model, electrons return to their parent ions and emit photons when driven by a linearly polarized laser. In localized systems, adding ellipticity can significantly reduce the probability of collision between electrons and parent ions by deviating the trajectory. However, due to the nonlocality in crystals, the change of harmonic intensity with ellipticity is not significant. The results we show are different from those in crystals, indicating that electrons have significant localization in this anisotropic disordered system.

On the basis of the model in Fig. 1(a), we further increase the disorder degree of molecular arrangement. The distribution of molecules is random in both the x and y directions, but

the molecular axes remain parallel to the y axis, as shown in Fig. 8(a). This arrangement is similar to nematic liquid crystal. Compared with that in Fig. 1, the molecular center in this configuration adds the disorder degree in y direction, and the layered population disappears. The parameters of the laser are the same as those in Fig. 1. The harmonic spectra show some similarities to those in Fig. 1, but with a lower harmonic yield and clearer harmonic peaks. With the increase of disorder, collisions become more frequent, so the attenuation of harmonic intensities is expected. There is a plateau similar to that existing in gas HHG in the range from 13th–23rd in Fig. 8(b). After the 23rd order, the harmonics rapidly decays to a noise level, which are difficult to observe in the experiment. We regard the 23rd order as cutoff, and here we do not pay

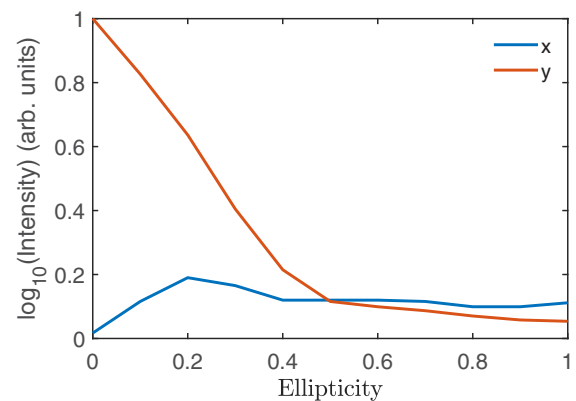
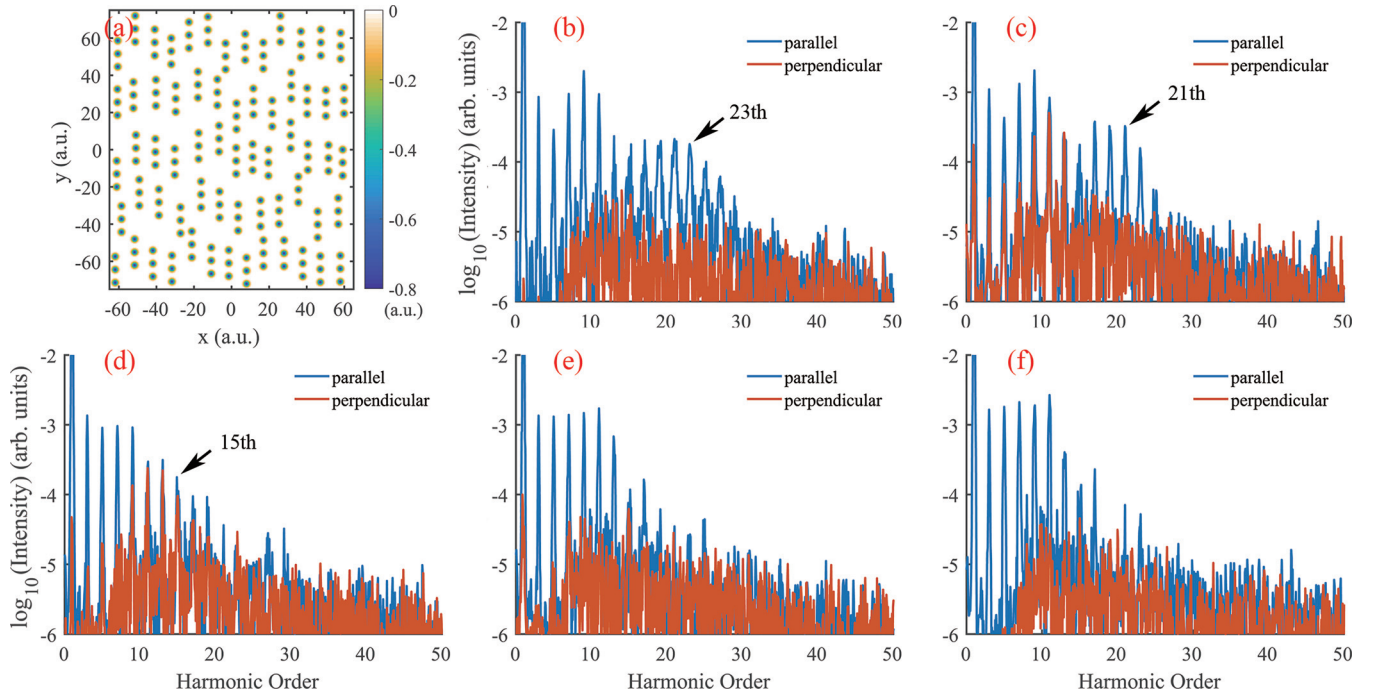
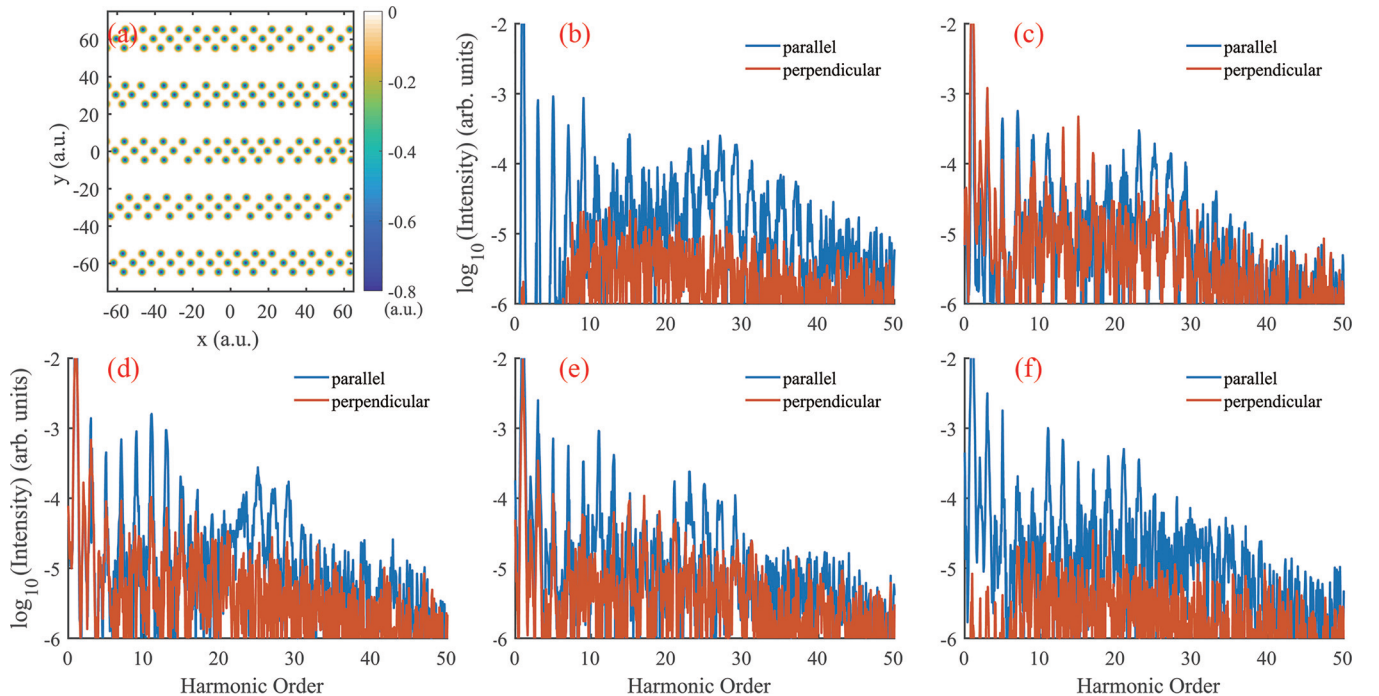


FIG. 7. The blue and red lines show the variation of harmonic intensity in x and y directions with the ellipticity ε , respectively.

FIG. 8. Same as Fig. 1, except that the position of the molecules is disordered in the y direction.

attention to the weak harmonics behind it. According to the semiclassical three-step model of gas HHG, the cutoff energy $3.17U_p + I_p$ is about the 31st order, where $U_p = E_0^2/(4\omega^2)$ is ponderomotive potential, $I_p = 4.6$ eV is the ionization energy of the highest occupied state. This is different from the cutoff position of the harmonic spectra, because of the environmental effect. As the polarization angle θ increases, the cutoff energy in the plateau decreases from 23rd ($\theta = 0$) to 21st

($\theta = \pi/8$) until 15th ($\theta = \pi/4$) order. As can be seen from Fig. 4, the average momentum of tunneling electrons decays during the scattering process, which means that the number of electrons with larger momentum decreases. It is necessary to note that there may be a few returned electrons that retain enough energy close to $3.17U_p$, but the harmonic intensity of their contribution is so low that they are almost submerged in noises.

FIG. 9. Same as Fig. 1, except that the molecular axis rotates $\pi/4$.

A model of a different configuration is depicted in Fig. 9(a). In this configuration, although the molecules are still arranged in layers, the molecular axis of the molecules rotates by $\pi/4$ in comparison to the configuration shown in Fig. 1. One distinguished feature of this configuration is that harmonics near the 27th order are enhanced, except when $\theta = \pi/2$. This observation highlights the dependence of harmonic generation mechanism on the polarization angle of the laser. The enhancement of harmonics may be related to the scattering of electrons between layers. Due to the molecular axis tilt and the spacing between layers is unchanged, the gap between molecules increases, allowing for greater possible movement range of electrons. When the laser is driven along the x axis ($\theta = \pi/2$), electrons collide with adjacent molecules in the layer almost immediately after they are tunneled out, resulting in weak interband harmonic intensity in the plateau and no enhancement of the harmonic near the 27th order. This behavior reflects the dependence of the harmonic generation mechanism on the polarization angle of the laser.

IV. CONCLUSION

In summary, we perform calculations of HHG in two-dimensional anisotropic disordered systems that are similar to liquid crystals. Our findings suggest that the high-order

harmonics induced by linearly polarized lasers reflect the differences in the scattering probability of tunneling electrons moving along different directions. We further show that intermolecular interactions cause the electron trajectories to be deflected, resulting in a time delay between high-order harmonics in two orthogonal directions in the plane of laser polarization. Unlike previous studies that rely on Berry curvature and other mechanisms, we find that the deflection mechanism of this electron trajectory is due to disorder and anisotropy. Moreover, during the HHG process, changes in the electron velocity occur rapidly, resulting in corresponding changes in the polarization properties of EUV coherent radiation in suboptical cycles. Therefore, the polarization characteristics of harmonics could be used to distinguish short and long trajectories. Our study offers insights into the ultrafast control of electron dynamics and polarization properties, making a valuable contribution to the understanding of ultrafast dynamics in anisotropic disordered systems, especially liquid crystals.

ACKNOWLEDGMENTS

This work is supported by the National Natural Science Foundation of China (Grant No. 12204492), the CAS Project for Young Scientists in Basic Research (Grant No. YSBR-059), and the K. C. Wong Education Foundation (Grant No. GJTD-2019-15).

-
- [1] W. Kaiser and C. G. B. Garrett, *Phys. Rev. Lett.* **7**, 229 (1961).
 - [2] L. V. Keldysh, *J. Exp. Theor. Phys.* **47**, 1945 (1964) [*Sov. Phys. JETP* **20**, 1307 (1965)].
 - [3] F. H. M. Faisal, *J. Phys. B* **6**, L89 (1973).
 - [4] A. McPherson, G. Gibson, H. Jara, U. Johann, T. S. Luk, I. A. McIntyre, K. Boyer, and C. K. Rhodes, *J. Opt. Soc. Am. B* **4**, 595 (1987).
 - [5] P. B. Corkum, *Phys. Rev. Lett.* **71**, 1994 (1993).
 - [6] M. Lewenstein, P. Balcou, M. Y. Ivanov, A. L'Huillier, and P. B. Corkum, *Phys. Rev. A* **49**, 2117 (1994).
 - [7] P. M. Paul, E. S. Toma, P. Breger, G. Mullot, F. Augé, P. Balcou, H. G. Muller, and P. Agostini, *Science* **292**, 1689 (2001).
 - [8] K. A. Pronin and A. D. Bandrauk, *Phys. Rev. Lett.* **97**, 020602 (2006).
 - [9] S. Ghimire, A. D. DiChiara, E. Sistrunk, P. Agostini, L. F. DiMauro, and D. A. Reis, *Nature Phys.* **7**, 138 (2011).
 - [10] G. Vampa, C. R. McDonald, G. Orlando, D. D. Klug, P. B. Corkum, and T. Brabec, *Phys. Rev. Lett.* **113**, 073901 (2014).
 - [11] Y. S. You, M. Wu, Y. Yin, A. Chew, X. Ren, S. Gholam-Mirzaei, D. A. Browne, M. Chini, Z. Chang, K. J. Schafer, M. B. Gaarde, and S. Ghimire, *Opt. Lett.* **42**, 1816 (2017).
 - [12] T. T. Luu and H. J. Wörner, *Phys. Rev. A* **98**, 041802(R) (2018).
 - [13] B. Xue, Y. Tamaru, Y. Fu, H. Yuan, P. Lan, O. D. Mücke, A. Suda, K. Midorikawa, and E. J. Takahashi, *Ultrafast Sci.* **2021**, 9828026 (2021).
 - [14] P. Agostini, F. Fabre, G. Mainfray, G. Petite, and N. K. Rahman, *Phys. Rev. Lett.* **42**, 1127 (1979).
 - [15] L. Arissian, C. Smeenk, F. Turner, C. Trallero, A. V. Sokolov, D. M. Villeneuve, A. Staudte, and P. B. Corkum, *Phys. Rev. Lett.* **105**, 133002 (2010).
 - [16] R. Boge, C. Cirelli, A. S. Landsman, S. Heuser, A. Ludwig, J. Maurer, M. Weger, L. Gallmann, and U. Keller, *Phys. Rev. Lett.* **111**, 103003 (2013).
 - [17] M. Klaiber, K. Z. Hatsagortsyan, and C. H. Keitel, *Phys. Rev. Lett.* **114**, 083001 (2015).
 - [18] E. E. Serebryannikov and A. M. Zheltikov, *Phys. Rev. Lett.* **116**, 123901 (2016).
 - [19] P. Wessels *et al.*, *Commun. Phys.* **1**, 32 (2018).
 - [20] S. Eckart *et al.*, *Phys. Rev. Lett.* **121**, 163202 (2018).
 - [21] N. Tancogne-Dejean and A. Rubio, *Sci. Adv.* **4**, eaao5207 (2018).
 - [22] G. Ndashimiye, S. Ghimire, M. Wu, D. A. Browne, K. J. Schafer, M. B. Gaarde, and D. A. Reis, *Nature (London)* **534**, 520 (2016).
 - [23] G. Vampa, T. J. Hammond, N. Thiré, B. E. Schmidt, F. Légaré, C. R. McDonald, T. Brabec, and P. B. Corkum, *Nature (London)* **522**, 462 (2015).
 - [24] S. Ghimire *et al.*, *J. Phys. B* **47**, 204030 (2014).
 - [25] N. Yoshikawa, T. Tamaya, and K. Tanaka, *Science* **356**, 736 (2017).
 - [26] G. Vampa *et al.*, *Nature Phys.* **13**, 659 (2017).
 - [27] J. Li, X. Zhang, S. Fu, Y. Feng, B. Hu, and H. Du, *Phys. Rev. A* **100**, 043404 (2019).
 - [28] Y. S. You, Y. Yin, Y. Wu, A. Chew, X. Ren, F. Zhuang, S. Gholam-Mirzaei, M. Chini, Z. Chang, Y. S. You, and S. Ghimire, *Nature Commun.* **8**, 724 (2017).
 - [29] J. Q. Liu and X. B. Bian, *Phys. Rev. Lett.* **127**, 213901 (2021).
 - [30] T. T. Luu, Z. Yin, A. Jain, T. Gaumnitz, Y. Pertot, J. Ma, and H. J. Wörner, *Nature Commun.* **9**, 3723 (2018).
 - [31] A. W. Zeng and X. B. Bian, *Phys. Rev. Lett.* **124**, 203901 (2020).

- [32] M. A. L. Marques, A. Castro, and G. F. Bertsch, [Comput. Phys. Commun.](#) **151**, 60 (2003).
- [33] A. Castro, H. Appel, M. Oliveira, C. A. Rozzi, X. Andrade, F. Lorenzen, M. A. L. Marques, E. K. U. Gross, and A. Rubio, [Phys. Status Solidi \(b\)](#) **243**, 2465 (2006).
- [34] X. Andrade *et al.*, [Phys. Chem. Chem. Phys.](#) **17**, 31371 (2015).
- [35] M. Wilson, [Int. Rev. Phys. Chem.](#) **24**, 421 (2005).
- [36] C. M. Care and C. J. Cleaver, [Rep. Prog. Phys.](#) **68**, 2665 (2005).
- [37] M. P. Allen, [Lect. Notes Phys.](#) **704**, 191 (2006).
- [38] C. Chandre, S. Wiggins, and T. Uzer, [Physica D \(Amsterdam\)](#) **181**, 171 (2003).
- [39] H. Liu, Y. Li, Y. S. You, S. Ghimire, T. F. Heinz, and D. A. Reis, [Nature Phys.](#) **13**, 262 (2017).
- [40] T. T. Luu and H. J. Wörner, [Nature Commun.](#) **9**, 916 (2018).